JCTC Journal of Chemical Theory and Computation

Article

pubs.acs.org/JCTC

Assessing the Performance of CASPT2 and DFT Methods for the Description of Long, Multicenter Bonding in Dimers between Radical Ions

Marçal Capdevila-Cortada,* Jordi Ribas-Arino, and Juan J. Novoa

Departament de Química Física and IQTCUB, Facultat de Química, Universitat de Barcelona, Av. Diagonal 645, 08028 Barcelona, Spain

Supporting Information

ABSTRACT: The performance of a wide variety of density functionals for the description of long, multicenter bonding in dimers between radical ions has been addressed in this work. Results on interaction energies and equilibrium distances have been evaluated through pure GGA and meta-GGA, hybrid, RSH, and double hybrid functionals. Grimme's dispersion corrections have also been assessed. All results are systematically analyzed and compared for the π-$[TCNE]_2^{2-}$, π-$[TTF]_2^{2+}$, π-$[TCNB]_2^{2-}$, and π-$[TCNP]_2^{2-}$ dimers. The DFT results are benchmarked against RASPT2 calculations based on large active spaces. It is shown that small active spaces do not quantitatively describe the interaction energy curves of these dimers. B97-D3(BJ) turns to be the functional that best reproduces the finest RASPT2 results, while PBE-D3(BJ), B3LYP-D3(BJ), and M06-L also provide satisfactory results.

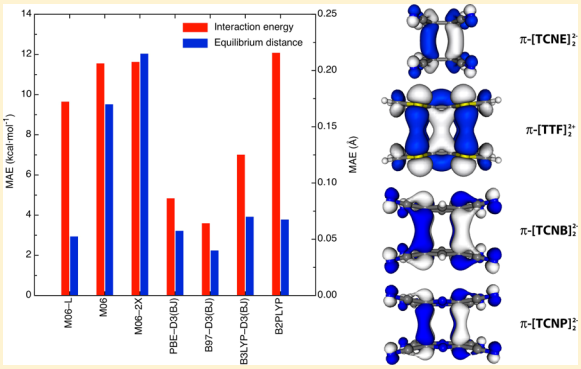

INTRODUCTION

Organic compounds with a large electron donor (acceptor) capability have been the subject of great interest over the last decades.[1] These compounds are commonly used in solids presenting conducting,[2] superconducting,[3] magnetic,[4] or other physical properties.[5] However, their mono-oxidized (reduced) form can dimerize resulting in a diamagnetic long, multicenter bonded entity, where the SOMOs of the radical ions overlap leading to doubly occupied bonding and an empty antibonding combination. Such long, multicenter bonds present spectroscopic similarities to covalent bonds but differ in their nature, strength, and equilibrium distance.[6] Isolated long bonded dimers of radical ions are metastable, with a small barrier toward dissociation, because the stabilization obtained by the bonding term (as a result of the double occupation of the SOMOs bonding combination) plus the dispersion term results in the presence of a minimum, although it is not large enough to defeat the Coulombic repulsion between the radical ions. However, they do form in the solid state and in low temperature solutions due to the interactions between the long bonded dimer and the adjacent counterions or solvent molecules, respectively, which overcome the repulsion between the radical ions that form the dimer.[7] Because their first characterization in salts of reduced tetracyanoethylene[8] (TCNE, whose π-$[TCNE]_2^{2-}$ diamagnetic dimers present an intermonomer distance of ~2.9 Å), several other radical ions have been shown to exhibit long, multicenter bonding, such as tetracyanobenzene (TCNB),[9] tetracyanopyrazine (TCNP),[10] and tetrathiafulvalene (TTF).[11] They have also been observed in zwitterionic π-$[TTF^{\delta+}\cdots TCNE^{\delta-}]$ charge-transfer dyads.[12]

Because of the multireference character of these long bonded dimers at the equilibrium distance range, second-order perturbation theory calculations on multireference wave functions are considered to be the best affordable method to accurately evaluate these interactions. Although their nature can be qualitatively described by a minimum (2,2) active space,[7b,c] a recent study based on a VB description[13] suggests that π-$[TCNE]_2^{2-}$ requires a (6,4) active space, where the full π-space of the central C−C of both $[TCNE]^{\cdot-}$, parallel to the bonding axis, should be included to reach quantitative accuracy.[14] VB calculations also revealed significant contributions from charge-shift effects on π-$[TCNE]_2^{2-}$ long, multicenter bonding.[15] DFT methods are also frequently used on the modeling of such interactions, mainly the Minnesota set of functionals (more precisely, M05-2X,[16] M06-L,[17] M06,[18] and M06-2X)[17c,19] and previously B3LYP.[7c,d,8,10a,11,20] Yet, the correct description of di-ionic π-dimers presenting long, multicenter bonds by DFT methods is not straightforward due to their multireference character at the equilibrium range, even if density functionals tend to avoid symmetry breaking at equilibrium distances.[21]

Despite the common use of DFT to model such interactions, a systematic assessment of the performance of density functionals in this context is still missing. A first step toward this aim was done by Kertesz and co-workers, who recently

Received: November 26, 2013
Published: January 6, 2014

   dx.doi.org/10.1021/ct4010257 | J. Chem. Theory Comput. 2014, 10, 650−658

studied the performance of several density functionals compared to MRPT2(2,2) results on a neutral dithiadiazolyl long bonded π-dimer and its diselenadiazolyl analogue.[22] This study concludes that M06 is the best functional, among the ones used in the work, to properly describe this system. A similar study has been recently reported in a large group of neutral and monoionic charged π-dimers, although they excluded di-ionic long bonded π-dimers.[23]

The methodical DFT benchmark is not only missing but also a pressing issue in view of the fact that long, multicenter bonding has been observed in several supramolecular and large complex molecules with potential applications as room temperature molecular switches.[17c,24] It is clear that correlated wave function methods are unaffordable in these cases. Hence, the use of a proven reliable functional becomes essential on such large systems instead of dealing with resource-demanding CASPT2 calculations based on large active spaces.

In this work, we provide a systematic study on the description of long, multicenter bonds between charged radicals by means of CASPT2 (RASPT2) calculations based on various CASSCF (RASSCF) active spaces. Furthermore, we benchmark a wide class of density functionals, considering GGA and meta-GGA pure and hybrid functionals, long-range corrected hybrid functionals, double hybrid functionals, and empirical dispersion corrections. The results are systematically carried out and compared for the π-$[TCNE]_2^{2-}$, π-$[TCNB]_2^{2-}$, and π-$[TCNP]_2^{2-}$ dianion dimers and the π-$[TTF]_2^{2+}$ dication dimer (Scheme 1). On the whole, it will be proven that density functional methods can successfully reproduce CASPT2 results.

Scheme 1. Chemical Structures of TCNE, TTF, TCNB, and TCNP Molecules

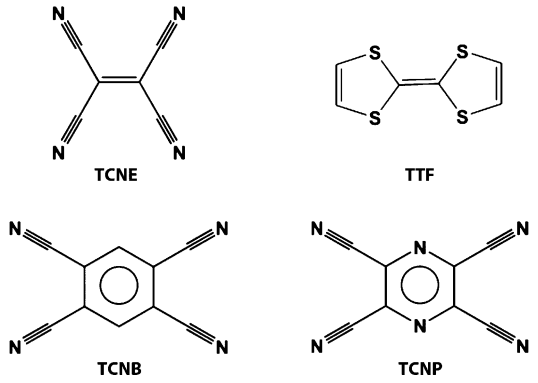

METHODOLOGY

First, the commonly used (2,2) active space has been tested against larger active spaces in the π-$[TCNE]_2^{2-}$ and π-$[TCNP]_2^{2-}$ dianion dimers. This active space results from the bonding and antibonding combination of the SOMO of both monomers. Then, according to the literature, the first larger active space that has been assessed comprises the direct π-space parallel to the bonding axis, that is, (6,4) and (14,12) for the π-$[TCNE]_2^{2-}$ and π-$[TCNP]_2^{2-}$ dimers, respectively. The second larger active space considered is (22,20) for the π-$[TCNE]_2^{2-}$ dimer and (30,28) for the π-$[TCNP]_2^{2-}$ dimer. This results from also considering the π-space of the cyano groups, and it is treated at the RASSCF/RASPT2 level. All multireference calculations are performed on B3LYP/6-31+G(d) optimum geometries.

This work analyzes 23 density functionals, including a standard generalized gradient approximation (GGA), meta-GGA, hybrid GGA, hybrid meta-GGA, range-separated hybrid (RSH), and double hybrid functionals, which are systematically compared to the RASPT2 results. Grimme's empirical dispersion corrections D2, D3, and D3(BJ) are also considered. PBE[25] and BP86[26] are the only pure GGA functional among the list of functionals considered herein. The hybrid GGA functionals B3LYP[27] and BH&HLYP[28] (as implemented in Gaussian09) and the hybrid meta-GGA functional BMK[29] are also included in the benchmark. The RSH functionals CAM-B3LYP,[30] HSE06,[31] and ωB97X[32] are considered. The D2, D3, and D3(BJ) Grimme's empirical dispersion are added to the pure GGA PBE and the hybrid B3LYP functionals, whereas D2 is also added to the RSH ωB97X. In addition, B97-D2,[33] B97-D3,[34] and B97-D3(BJ)[35] are also considered. Finally, four Minnesota functionals are included in this work, the pure meta-GGA M06-L,[36] hybrid meta-GGA functionals M06[37] and M06-2X,[36] and RSH M11.[38] The double hybrid functional B2PLYP[39] has also been considered for the π-$[TCNE]_2^{2-}$ and π-$[TTF]_2^{2+}$ dimers. Table 1 summarizes the information about the density functionals used in this work. A (75,305) Lebedev[40] grid is used in all functionals besides M06-L, M06, M06-2X, and M11, for which more precise (99,590) and (150,974) grids are also considered.

Table 1. Density Functionals Used in This Work

density functional	type	% HF exch.	ref.
PBE	GGA	–	25
PBE-D2	GGA	–	33
PBE-D3	GGA	–	34
PBE-D3(BJ)	GGA	–	35
BP86	GGA	–	26
M06-L	meta-GGA	–	36
B97-D2	GGA	–	33
B97-D3	GGA	–	34
B97-D3(BJ)	GGA	–	35
B3LYP	hybrid GGA	20	27
B3LYP-D2	hybrid GGA	20	33
B3LYP-D3	hybrid GGA	20	34
B3LYP-D3(BJ)	hybrid GGA	20	35
BH&HLYP	hybrid GGA	50	28
BMK	hybrid meta-GGA	42	29
M06	hybrid meta-GGA	27	37
M06-2X	hybrid meta-GGA	54	37
CAM-B3LYP	range-separated hybrid	19/65[a]	30
HSE06	range-separated hybrid	25/0[a]	31
ωB97X	range-separated hybrid	15.8/100[a]	32
ωB97X-D2	range-separated hybrid	22.2/100[a]	41
M11	range-separated hybrid	42.8/100[a]	38
B2PLYP	double hybrid	53 (27)[b]	39

[a]HF exchange percentage at short-range/long-range. [b]PT2 correlation percentage given within parentheses.

Interaction energies are obtained from ground-state relaxed potential energy surfaces, as a function of the intermonomer distance (r: in π-$[TCNE]_2^{2-}$ and π-$[TTF]_2^{2+}$, this distance is defined as the distance between both centers of mass of the central C−C carbons, while in π-$[TCNB]_2^{2-}$ and π-$[TCNP]_2^{2-}$ dimers, it is set between the centers of mass of each aromatic

dx.doi.org/10.1021/ct4010257 | J. Chem. Theory Comput. 2014, 10, 650−658

ring). All geometries are constrained to D_{2h} point group symmetry. The broken-symmetry approach is used within the unrestricted Kohn−Sham formalism (UDFT) in order to converge to open-shell singlet ground states (further details are given in the Supporting Information). The RASPT2 reference values are based on active spaces formed from the full π-space parallel to the bonding axis of each dimer, keeping a (2,2) in each RAS2 (i.e., (22,2,2;10,2,8)[42] for π-$[TCNE]_2^{2-}$, (26,2,2;12,2,6) for π-$[TTF]_2^{2+}$, and (30,2,2;14,2,12) for both π-$[TCNB]_2^{2-}$ and π-$[TCNP]_2^{2-}$). Previous calculations on $[TCNE]^{\cdot-}$ and $[TTF]^{\cdot+}$ monomers are also based on such actives spaces.[43]

The standard 6-31+G(d) Pople basis set is used in all calculations, besides in the Basis Set Analysis section, where the 6-31G(d), 6-311G(d,p), 6-311+G(d,p), and 6-311+G(2d,p) basis sets are also used.[44] All interaction energy values are BSSE corrected by means of the Counterpoise method.[45] The standard IPEA Hamiltonian and the Cholesky decomposition of two-electron integrals were used on all multireference calculations.[46] DFT calculations were done using the Gaussian09 package,[47] while multireference calculations were carried out with the Molcas7.6 package.[48]

RESULTS AND DISCUSSION

1. Reference CASPT2/RASPT2 Interaction Energy Curves. Interaction energy curves are performed with several active spaces for the π-$[TCNE]_2^{2-}$ and π-$[TCNP]_2^{2-}$ dianion dimers (Figure 1) not only to assess the validity of the minimum (2,2) active space but also to analyze the achievement of an active space convergence. Three more active spaces are considered for the π-$[TCNE]_2^{2-}$ dimer, (6,4), and (22,20) (see Methodology section), for which two variations of the RAS active space have been chosen, (22,2,2;10,2,8) and (22,2,2;8,4,8). The former results are from considering a (2,2) active space as the RAS2, while the latter are from considering a (6,4) active space as the RAS2. The CASPT2-(2,2) curve exhibits a minimum at ∼2.5 Å, slightly overestimating the interaction energy by about 2.5 kcal mol^{-1} compared to the RASPT2(22,2,2;8,4,8). The largest active space shows a minimum at around 2.7 Å with an interaction energy value of ∼37 kcal mol^{-1}.[49] The minimum region is accurately described with the CASPT2(6,4) curve, which is only slightly shifted from the optimum distance (<0.1 Å). The RASPT2(22,2,2;10,2,8) curve almost overlaps the RASPT2-(22,2,2;8,4,8), although it slightly overbinds the minimum region. On the other hand, the dissociation region perfectly matches with both (22,20) RASPT2 active spaces, while the smaller active spaces underestimate the interaction energy by about 2 kcal mol^{-1}. It thus means that the π-space of the cyano groups increases significantly in the dissociation region, in agreement with the geometry evolution, which gradually becomes planar as long as the intermolecular distance increases (note that the four curves finally converge at larger distances; Figure S1, Supporting Information). Moreover, each CASSCF/RASSCF wave function has been analyzed in terms of its natural orbitals occupation (Table S1, Supporting Information). The bonding and antibonding combinations of the SOMOs have an occupation of 1.76 and 0.24 at the equilibrium distance, respectively, on the (2,2) active space, while they reach a value of 1.81 and 0.23 on the largest RAS active space. The (6,4) active space almost shows the same occupation (1.82 and 0.21) as the largest RAS, providing a similar result to the smaller RAS active space. The other orbitals have an occupation number greater than 1.96 for the occupied orbitals and around 0.03−0.04 for the virtual orbitals. On the whole, we can state that the wave function is accurately described at the equilibrium range with a (6,4) active space, although (2,2) already provides a good enough qualitative description.

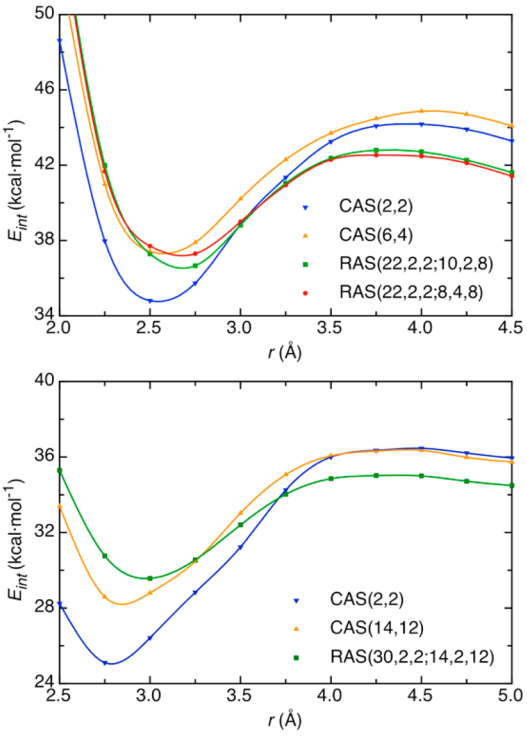

Figure 1. Interaction energy curves for the π-$[TCNE]_2^{2-}$ (top) and π-$[TCNP]_2^{2-}$ (bottom) dimers, computed at the CASPT2(RASPT2)/6-31+G(d) level with various active spaces. All values are BSSE corrected.

The close similarity of the interaction curves obtained with both (22,20) RASPT2 spaces, together with the small deviation observed in the CASPT2(6,4) curve, constitutes a strong piece of evidence that the (22,20) multireference calculations carried out on the π-$[TCNE]_2^{2-}$ dimer are converged with respect to the size of the active space. The same argument applies when considering the natural orbitals occupation collected in Table S1 of the Supporting Information. In addition, it should be mentioned that, to the best of our knowledge, the (22,20) active space is the largest active space ever used for the π-$[TCNE]_2^{2-}$ dimer. Hence, the green and red curves of Figure 1 (top) should be viewed as the best benchmark interaction curves thus far reported for this long, multicenter bonded dimer.[50]

The (2,2) active space is compared to the (14,12) and (30,28) active spaces for the π-$[TCNP]_2^{2-}$ dimer. The (30,28) active space corresponds to a RASPT2(30,2,2;14,2,12) calculation, which considers a (2,2) active space as the RAS2. Because only one restricted active space is now considered, the (30,28) notation will be used to refer to the (30,2,2;14,2,12) RAS. Figure 1 (bottom) shows for the π-$[TCNP]_2^{2-}$ dimer the same trends exhibited by the π-$[TCNE]_2^{2-}$ dimer. The CASPT2(2,2) curve overbinds the minimum region by about 5 kcal mol^{-1}, and it is shifted to a shorter equilibrium distance. The CASPT2(14,12) is in better agreement compared to the RASPT2(30,28) curve, reaching a close result in energy and distance terms, although the dissociation region is under-

dx.doi.org/10.1021/ct4010257 | J. Chem. Theory Comput. 2014, 10, 650−658

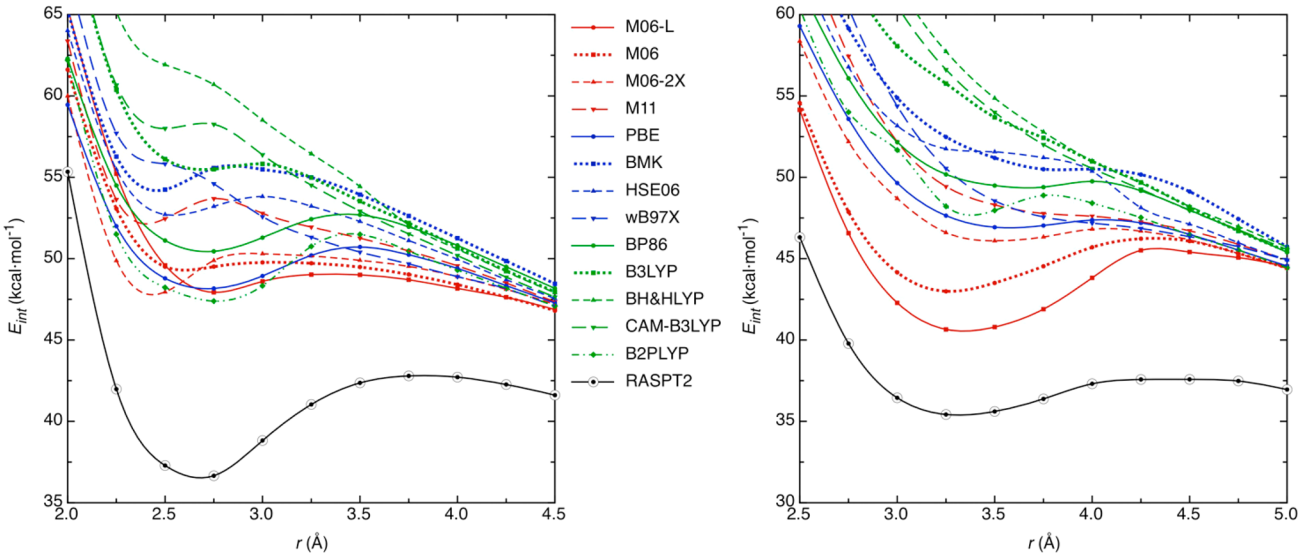

Figure 2. Interaction energy curves for the π-$[TCNE]_2^{2-}$ (left) and π-$[TTF]_2^{2+}$ (right) dimers computed with several density functionals. RASPT2 serves as the reference value. All values are BSSE corrected, and the 6-31+G(d) basis set was used. An enlarged view of the density functionals region for the π-$[TCNE]_2^{2-}$ dimer is found in Figure S2 of the Supporting Information.

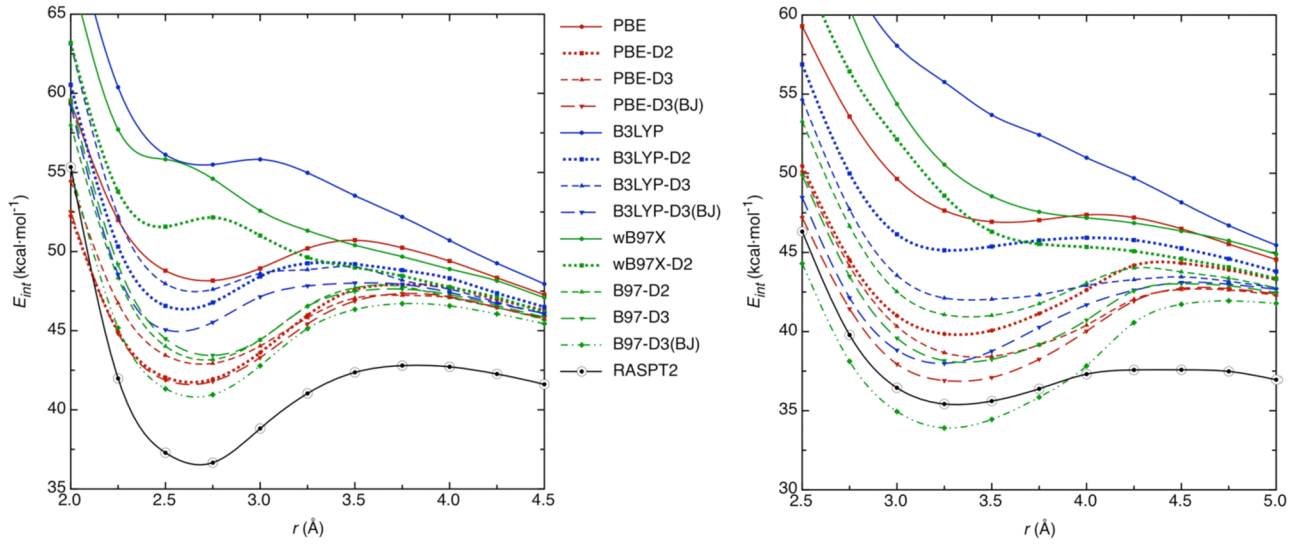

Figure 3. Interaction energy curves for the π-$[TCNE]_2^{2-}$ (left) and π-$[TTF]_2^{2+}$ (right) dimers computed with PBE, B3LYP, ωB97X, and B97 density functionals with D2, D3, and D3(BJ) Grimme's dispersion corrections. RASPT2 serves as the reference value. All values are BSSE corrected, and the 6-31+G(d) basis set was used.

estimated by about 2 kcal mol^{-1}. Similarly, the (30,28) active space here performed is, to the best of our knowledge, the best benchmark interaction curve reported so far for the description of the π-$[TCNP]_2^{2-}$ dimer.[S1]

Therefore, it can be concluded that to accurately describe the long bond mestastable minimum the direct π-space parallel to the bonding axis should be added to the (2,2) active space. However, because the geometry of each monomer gradually becomes planar when the intermonomer distance is increased, the π-space of the cyano groups (parallel to the bonding axis) should be also included along the dissociation regime.

2. Density Functionals Assessment. A total of 23 density functionals are evaluated in the present section in terms of interaction energies compared to the RASPT2 reference values (see Methodology section for the active spaces description). Interaction energy curves of a first subset of density functionals for the π-$[TCNE]_2^{2-}$ and π-$[TTF]_2^{2+}$ dimers are plotted in Figure 2. As shown in the previous section, the RASPT2 curve for the π-$[TCNE]_2^{2-}$ dimer exhibits a minimum at ~2.7 Å of about 37 kcal mol^{-1}, around 11 kcal mol^{-1} more stable than the most stable DFT curves. Among them, the B2PLYP, M06-L, and PBE functionals show the best performance, providing a minimum at about the same intermonomer distance. M06 and M06-2X exhibit a minimum at similar energies, although they underestimate the equilibrium distance by 0.1−0.3 Å. On the other hand, BP86 provides a minimum at the same intermonomer distance but is 3 kcal mol^{-1} less stable than the B2PLYP, M06-L, and PBE functionals. M11, HSE06, BMK, B3LYP, and CAM-B3LYP predict a minimum at slightly lower equilibrium distances about 5−10 kcal mol^{-1} less stable than the M06-L and PBE functionals. BH&HLYP and ωB97X fail in reproducing any bound minimum. Note also that the barrier toward dissociation is underestimated by all functionals, with B2PLYP, PBE, and BP86 providing the higher barrier.

dx.doi.org/10.1021/ct4010257 | J. Chem. Theory Comput. 2014, 10, 650−658

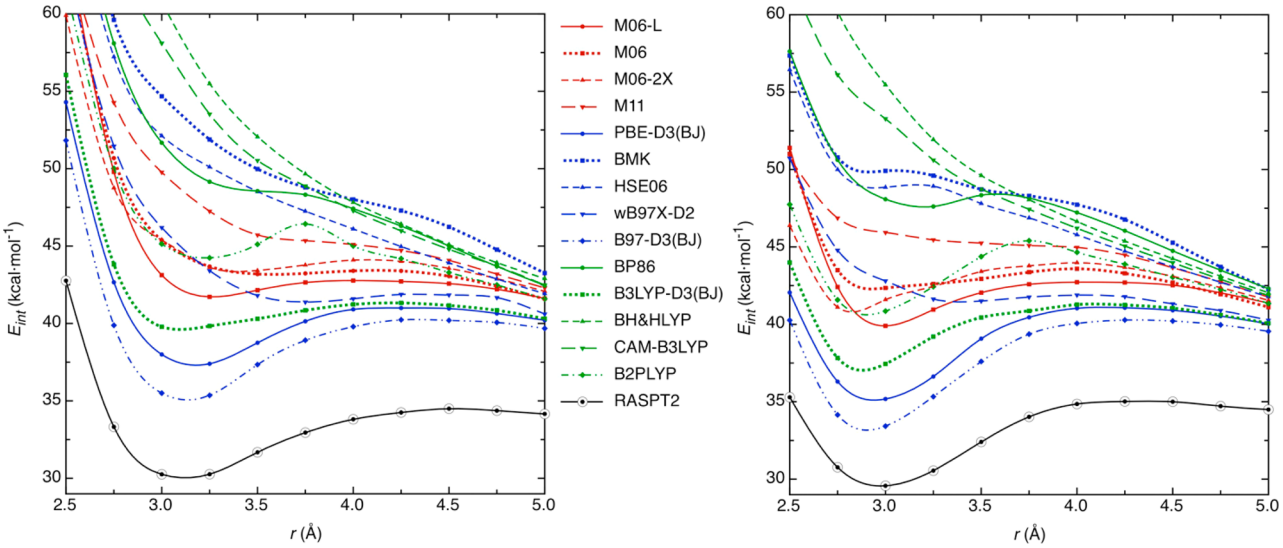

Figure 4. Interaction energy curves for the π-$[TCNB]_2^{2-}$ (left) and π-$[TCNP]_2^{2-}$ (right) dimers computed with several density functionals. RASPT2 serves as the reference value. All values are BSSE corrected, and the 6-31+G(d) basis set was used.

For the π-$[TTF]_2^{2+}$ dimer, the RASPT2 curve exhibits a minimum of 35 kcal mol^{-1} at about 3.3 Å. The M06-L functional provides a minimum at the same equilibrium distance only 5 kcal mol^{-1} less stable than the RASPT2 minimum. M06 also performs reasonably well and shows a minimum at ∼3.2 Å of about 43 kcal mol^{-1}. B2PLYP provides a bound dimer at ∼3.3 Å of around 48 kcal mol^{-1}. M06-2X, PBE, BP86, and BMK functionals exhibit a shallow minimum at slightly higher equilibrium distances of 6−10 kcal mol^{-1} less stable than the M06-L minimum. The other functionals are not able to reproduce a bound minimum for the π-$[TTF]_2^{2+}$ dimer. It is worth mentioning that the larger (150,974) grid must be used in conjunction with the Minnesota functionals (M06-L, M06, M06-2X, and M11) for both dimers in order to describe their dissociation regime (a comparative study between (75,305), (99,590), and (150,974) grids is given in Figures S3−S4 of the Supporting Information).

Grimme's empirical dispersion corrections D2, D3, and D3(BJ) are evaluated in Figure 3 on both π-$[TCNE]_2^{2-}$ and π-$[TTF]_2^{2+}$ dimers. D2, D3, and D3(BJ) corrections are added to PBE and B3LYP functionals, while D2 is added to ωB97X. Additionally, the B97-D2, B97-D3, and B97-D3(BJ) functionals are also included in Figure 3. The inclusion of dispersion corrections improves the results in all the cases studied here, always providing a minimum except for the ωB97X-D2 functional on the π-$[TTF]_2^{2+}$ dimer. D3(BJ) correction provides the best results compared to the RASPT2 curves, while D2 and D3 corrections perform similarly on PBE and B3LYP functionals. D2 reaches better results on the π-$[TCNE]_2^{2-}$ dimer and D3 on the π-$[TTF]_2^{2+}$ dimer, providing bound minima about 5−12 kcal mol^{-1} more stable than their parent curves. Among the 23 functionals considered, the functional that shows the best performance is B97-D3(BJ). It provides the most stable curve in both cases, being about 5 kcal mol^{-1} less stable than the RASPT2 curve for the π-$[TCNE]_2^{2-}$ dimer and overbinding the RASPT2 curve by about 1.5 kcal mol^{-1} for the π-$[TTF]_2^{2+}$ dimer. Also the equilibrium distance perfectly matches the RASPT2 one. Although PBE and B97 dispersion corrected curves reproduce well the barrier toward dissociation for the π-$[TCNE]_2^{2-}$ dimer, it is overestimated for the π-$[TTF]_2^{2+}$ one.

Figure 2's functionals are now assessed on π-$[TCNB]_2^{2-}$ and π-$[TCNP]_2^{2-}$ dimers. PBE-D3(BJ), B3LYP-D3(BJ), and ωB97X-D2 have been considered instead of their uncorrected parent functionals, and B97-D3(BJ) has also been added. Their interaction energy curves are plotted in Figure 4. The RASPT2 curve exhibits the metastable minimum at 3.1 Å of ∼30 kcal mol^{-1} for the π-$[TCNB]_2^{2-}$ dimer. B97-D3(BJ) is the density functional that better reproduces the RASPT2 results, providing a minimum at the same intermonomer distance and about 5 kcal mol^{-1} less stable. PBE-D3(BJ), B3LYP-D3(BJ), M06-L, and B2PLYP show a minimum at 3.1−3.2 Å ofabout 37, 40, 42, and 44 kcal mol^{-1}, respectively. The ωB97X-D2 functional also provides a minimum at around 42 kcal mol^{-1}, although it overestimates the equilibrium distance by 0.7 Å and its barrier toward dissociation is very small. The M06-2X and M06 curves exhibit very close results to ωB97X-D2, although 2 kcal mol^{-1} less stable. M11, BMK, HSE06, BP86, BH&HLYP, and CAM-B3LYP functionals are not able to provide a bound dimer. Note that, as expected, all functionals finally converge at large distances (Figure S5, Supporting Information).

A similar landscape is obtained for the π-$[TCNP]_2^{2-}$ dimer. B97-D3(BJ) is again the density functional that yields results in closer agreement with the RASPT2 curve, which provides a minimum at about 3.0 Å of 29.6 kcal mol^{-1}. The B97-D3(BJ) functional shows a minimum of 33.2 kcal mol^{-1} at 2.9 Å, 3 kcal mol^{-1} more stable than the minimum provided by the PBE-D3(BJ) functional, although the latter matches the 3.0 Å equilibrium distance of the RASPT2 curve. B3LYP-D3(BJ), M06-L, and B2PLYP show a minimum within the 2.9−3.0 Å range, 5−7 kcal mol^{-1} less stable than the B97-D3(BJ) functional. The M06-2X and M06 curves also present a minimum within a similar energy range, although at a slightly shorter equilibrium distance. The minimum observed in the ωB97X-D2 curve is within the same energy range than the previous functionals. However, its equilibrium distance is much higher (around 3.4 Å), and its barrier toward dissociation is lower than 0.5 kcal mol^{-1}. Also the HSE06 functional exhibits a minimum with a very low barrier toward dissociation, 20 kcal mol^{-1} less stable than the B97-D3(BJ) curve. The BP86 functional shows a minimum 0.2 Å higher than the RASPT2

dx.doi.org/10.1021/ct4010257 | J. Chem. Theory Comput. 2014, 10, 650−658

minimum, with a similar energy to that shown by the HSE06 curve. M11, BMK, BH&HLYP, and CAM-B3LYP curves do not present any minima at the studied distance range.

Figure 5 outlines the key concepts of the results obtained in this section. Among the density functionals employed on all

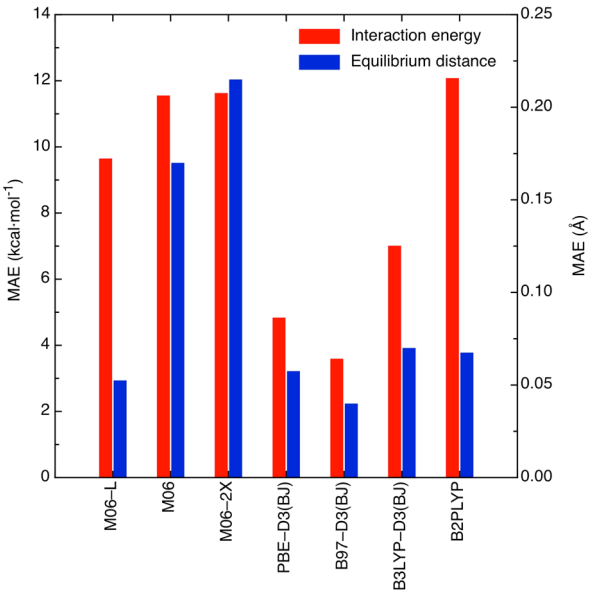

Figure 5. Interaction energy (red, left *y*-axis) and equilibrium distance (blue, right *y*-axis) MAEs of the seven functionals that provided a bound minimum on each four dimers compared to their RASPT2 reference curves. The 6-31+G(d) basis set was used.

four dimers, only seven provided a bound minimum in each system: M06-L, M06, M06-2X, PBE-D3(BJ), B97-D3(BJ), B3LYP-D3(BJ), and B2PLYP. Their mean absolute errors (MAE) against the minimum of each RASPT2 curve are shown in Figure 5 concerning their interaction energy and equilibrium distance. B97-D3(BJ) is the functional that best reproduces the RASPT2 results, both in energy and geometry terms, followed by the PBE-D3(BJ) density functional. M06-L provides slightly better equilibrium distances than PBE-D3(BJ), although its MAE in interaction energies almost reaches a value of 10 kcal mol^{-1} (twice the value of PBE-D3(BJ)). Dispersion corrections seem thus essential to successfully describe these interactions, either by means of empirical dispersion addition or using highly parametrized functionals. It is noteworthy that empirical dispersion corrections provide satisfactory results despite the fact that they were parametrized with ordinary van der Waals aggregates, whose equilibrium distance is longer than that of the systems herein studied. In this sense, it is not surprising that D3(BJ) performs better than D3/D2 because the use of the BJ-damping function avoids repulsive interatomic forces at short distances.[35] On the other hand, all RSH functionals here considered failed to reproduce the long bonded dimers interactions, even when empirical dispersion corrections are added.

3. Basis Set Effects. In this section, we evaluate the impact of the basis set on the interaction energy curves done so far for the π-$[TCNE]_2^{2-}$ dimer. CASPT2 curves based on CASSCF-(6,4) wave functions are shown in Figure 6, obtained with the 6-31G(d), 6-31+G(d), 6-311G(d), 6-311+G(d), and 6-311+G(2d) basis sets. The largest basis set, the 6-311+G(2d), provides the most stable curve, which is about 2.5 kcal mol^{-1}

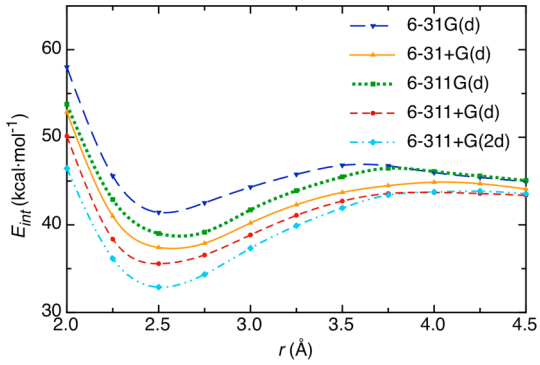

Figure 6. Interaction energy curves for the π-$[TCNE]_2^{2-}$ dimer obtained at CASPT2/CASSCF(6,4) level with several basis sets. All values are BSSE corrected.

more stable than the 6-311+G(d) basis set around the equilibrium distance. An interesting result is that diffuse functions become more important than increasing from double-ζ to triple-ζ basis sets. As a matter of fact, 6-311+G(2d), 6-311+G(d), and 6-31+G(d) provide very similar curves when the BSSE is not corrected (Figure S6, Supporting Information), but the larger the basis set is the more reduced is the BSSE (Figure S7, Supporting Information).

The 6-31+G(d) and the 6-311+G(d) basis sets are compared for the π-$[TCNE]_2^{2-}$ dimer with the seven best functionals outlined in the previous section (Figure 7). DFT curves are not

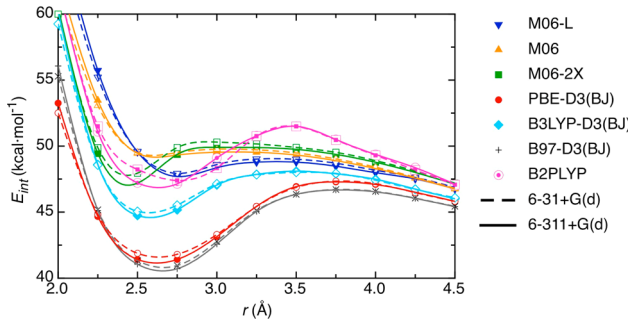

Figure 7. Interaction energy curves for the π-$[TCNE]_2^{2-}$ dimer obtained with several density functionals along with the 6-31+G(d) (dashed lines) and 6-311+G(d) (solid lines) basis sets. All values are BSSE corrected.

very basis set dependent when increasing from double-ζ to triple-ζ. In all cases, the energy difference between both curves is <1.0 kcal mol^{-1}, and they provide the same equilibrium distance, besides the B2PLYP double hybrid functional, on which the minimum is shifted ~0.2 Å. It thus follows that 6-31+G(d) is of sufficient quality for practical purposes (especially for large molecules or supramolecular aggregates).

4. Symmetry Breaking as a Tool To Reproduce Multireference Character in DFT. A discussion on how well DFT approaches the multireference character of the wave function is now presented. In the Introduction section, we pointed out the general trend of density functionals to avoid symmetry breaking at the equilibrium range. This issue is evaluated in Figure 8, where the occupation number of the HOMO of π-$[TCNE]_2^{2-}$ and π-$[TTF]_2^{2+}$ dimers is plotted as a function of the intermonomer distance. Figure 2's functionals are included in this analysis. A clear general trend is observed from Figure 8, where the higher percentage of HF exchange

dx.doi.org/10.1021/ct4010257 | J. Chem. Theory Comput. 2014, 10, 650−658

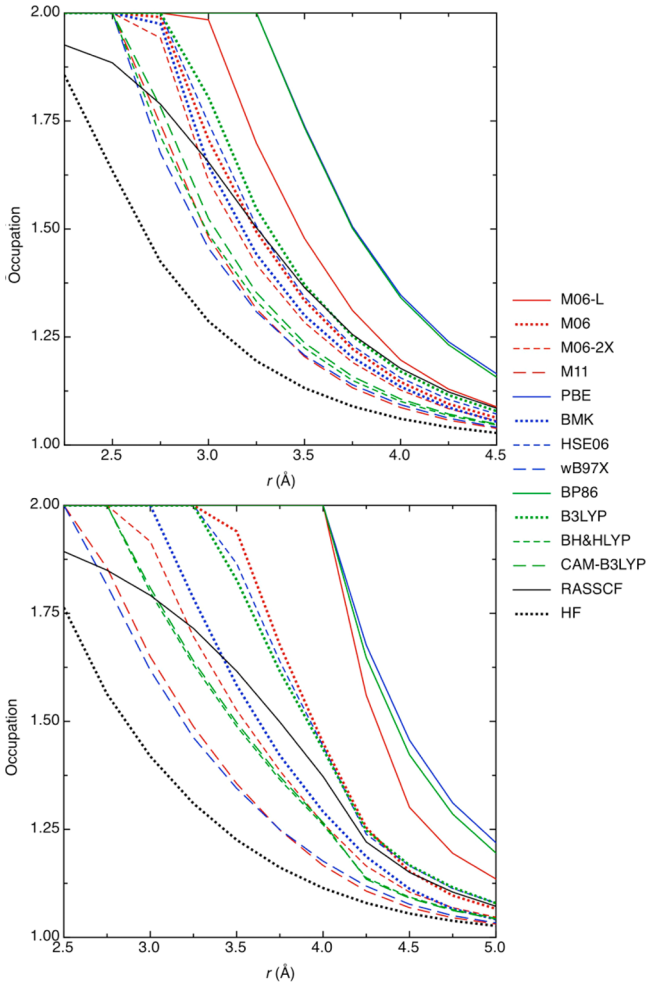

Figure 8. Occupation number of the HOMO of the π-$[TCNE]_2^{2-}$ (top) and π-$[TTF]_2^{2+}$ (bottom) dimers as a function of the intermonomer distance, obtained from the diagonalization of the first-order reduced density matrix from the UDFT calculations.

leads to a greater symmetry breaking. Hence, pure density functionals avoid symmetry breaking at the equilibrium range, while RSH functionals and hybrid functionals with high percentage of HF exchange, such as BH&HLYP or M06-2X, do not. On the other hand, B3LYP and M06 functionals, which contain a small amount of HF exchange, exhibit an average behavior. The behavior among RSH functionals strongly depends on the range parameter. The higher this value is the more long-range corrections the functional considers, and thus, a higher amount of HF exchange is included. Therefore, M11 and ωB97X (ω = 0.25 and 0.30 bohr^{-1}, respectively) exhibit symmetry breaking at remarkably short distances, while HSE06 (ω = 0.11 bohr^{-1}) and CAM-B3LYP (ω = 0.33 bohr^{-1}, with only 65% HF at long-range) present a similar behavior as hybrid functionals containing 30−50% of HF exchange. The same analysis can be carried out taking into account the LUMOs instead of the HOMOs (Figure S8, Supporting Information). Besides the closed-shell ground state at short distances, the smooth variation of the HOMO//LUMO occupation to the eventual 1.0//1.0 fully dissociated state is well reproduced by all density functionals, although hybrid functionals provide a closer match to the RASSCF occupations.

CONCLUSIONS

On the basis of a thorough computational study on four different model systems, we have gauged the performance of a wide variety of state-of-the-art density functionals when it comes to modeling the intriguing chemistry of long, multicenter bonding in dimers between radical ions. The DFT results have been benchmarked against CASPT2/RASPT2 calculations, which have been carried out based on different active spaces.

With reference to the wave function-correlated ab initio calculations, our investigation has revealed that the minimal (2,2) active space in CASPT2 calculations does not suffice to obtain quantitatively correct results. Indeed, the use of larger active spaces including the direct π-space parallel to the bonding axis is mandatory to accurately evaluate the interaction energy of the minima of the long, multicenter bonded dimers. The correct description of the energy barrier for dissociation of these dimers in turn requires even larger spaces that are tractable by means of RASSCF/RASPT2 calculations. In the case of a π-$[TCNE]_2^{2-}$ dimer, for instance, CASPT2(6,4) properly describes the interaction energy at the metastable minimum, while one has to resort to RASPT2(22,2,2;8,4,8) calculations to accurately deal with the dissociation energy barrier.

Concerning the performance of DFT, our benchmark study has demonstrated that the currently available density functionals tend to underestimate the interaction energy of long, multicenter-bonded dimers between charged radicals. In fact, some of the assessed functionals are not even able to predict the existence of the minima associated with the metastable dimers. The functional that best reproduces the CASPT2/RASPT2 interaction energy curves is the B97-D3(BJ) functional. For this particular functional, both the interaction energy of the dimers and their equilibrium distance are in reasonable agreement with CASPT2/RASPT2. Following the B97-D3(BJ) functional, PBE-D3(BJ), B3LYP-D3(BJ), and M06-L also provide notable results. The latter provides slightly better equilibrium distances albeit significantly worse interaction energies than the former two. Furthermore, our analysis has shown that going beyond a 6-31+G(d) basis set does not result in appreciably improved results when using the best functionals. It is thus concluded that this particular cost-efficient basis set offers enough quality for practical purposes. This is important in view of the fact that long, multicenter bonding has been recently observed in large complex molecules and supramolecular aggregates.

ASSOCIATED CONTENT

Supporting Information

Methodological details. Figure 1a extended at larger distances. Enlarged view of Figure 2a. π-$[TCNE]_2^{2-}$ and π-$[TTF]_2^{2+}$ dimers interaction energy curves obtained with several integration grids with the Minnesota functionals. Figure 4a extended at larger distances. BSSE-uncorrected interaction energy curves for the π-$[TCNE]_2^{2-}$ dimer obtained at CASPT2 level with several basis sets. BSSE curves for the π-$[TCNE]_2^{2-}$ dimer obtained at CASPT2 level with several basis sets. Figure 8 analogue with LUMO orbitals instead. Natural orbitals occupation of the π-$[TCNE]_2^{2-}$ dimer obtained with several active spaces. This material is available free of charge via the Internet at http://pubs.acs.org.

AUTHOR INFORMATION

Corresponding Author

*E-mail: m.capdevila@ub.edu.

Notes

The authors declare no competing financial interest.

ACKNOWLEDGMENTS

The work was financially supported by the MINECO of Spain (MAT2011-25972) and Generalitat de Catalunya (2009-SGR-1203). We also thank CESCA and BSC for their generous allocation of computer time in their facilities. J.R-A gratefully acknowledges the Spanish Government for a "Ramón y Cajal" contract.

REFERENCES

(1) (a) Miller, J. S. *Angew. Chem., Int. Ed.* **2006**, *45*, 2508. (b) Wudl, F. *Acc. Chem. Res.* **1984**, *17*, 227. (c) Ferraris, J.; Cowan, D. O.; Walatka, V.; Perlstein, J. H. *J. Am. Chem. Soc.* **1973**, *95*, 948.

(2) Ferraro, J. R.; Williams, J. M. *Introduction to Synthetic Electrical Conductors*; Academic Press: Orlando, 1987; pp 8−80.

(3) Ishiguro, T.; Yamaji, K. *Organic Superconductors*; Spinger-Verlag: Berlin, 1990; pp 99−156.

(4) (a) Kahn, O. *Molecular Magnetism*; Wiley-VCH: New York, 1993; pp 287−332. (b) Miller, J. S.; Epstein, A. *Angew. Chem., Int. Ed.* **1994**, *33*, 385. (c) Lahti, P. M., Ed.; *Magnetic Properties of Organic Materials*; Marcel Dekker: New Yok, 1999; pp 427−629; (d) Itoh, K.; Kinoshita, M. *Molecular Magnetism: New Magnetic Materials*; Kodansha: Tokyo, 2000; pp 207−288; (e) Veciana, J. *π-Electron Magnetism: From Molecules to Magnetic Materials*, Springer: Berlin, 2001; pp 33−60.

(5) Novoa, J.; Braga, D.; Addadi, L., Eds.; *Engineering of Crystalline Materials Properties*; Springer: Dordrecht, 2007; pp 375−400.

(6) Miller, J. S.; Novoa, J. J. *Acc. Chem. Res.* **2007**, *40*, 189.

(7) (a) Jakowski, J.; Simons, J. *J. Am. Chem. Soc.* **2003**, *125*, 16089. (b) Jung, Y.; Head-Gordon, M. *Phys. Chem. Chem. Phys.* **2004**, *6*, 2008. (c) Garcia-Yoldi, I.; Mota, F.; Novoa, J. J. *J. Comput. Chem.* **2007**, *28*, 326. (d) Garcia-Yoldi, I.; Miller, J. S.; Novoa, J. J. *J. Phys. Chem. A* **2007**, *111*, 8020.

(8) (a) Novoa, J. J.; Lafuente, P.; Del Sesto, R. E.; Miller, J. S. *Angew. Chem., Int. Ed.* **2001**, *40*, 2540. (b) Del Sesto, R. E.; Miller, J. S.; Lafuente, P.; Novoa, J. J. *Chem.—Eur. J.* **2002**, *8*, 4894. (c) Novoa, J. J.; Lafuente, P.; Del Sesto, R. E.; Miller, J. S. *CrystEngComm* **2002**, *4*, 373.

(9) Trifonov, A. A.; Gudilenkov, I. D.; Fukin, G. K.; Cherkasov, A. V.; Larionova, J. *Organometallics* **2009**, *28*, 3421.

(10) (a) Novoa, J. J.; Stephens, P. W.; Weerasekare, M.; Shum, W. W.; Miller, J. S. *J. Am. Chem. Soc.* **2009**, *131*, 9070. (b) Rosokha, S. V.; Lu, J.; Han, B.; Kochi, J. K. *New J. Chem.* **2009**, *33*, 545.

(11) Garcia-Yoldi, I.; Miller, J .S.; Novoa, J. J. *J. Phys. Chem. A* **2009**, *113*, 484.

(12) Capdevila-Cortada, M.; Novoa, J. J.; Bell, J. D.; Moore, C. E.; Rheingold, A. L.; Miller, J. S. *Chem.—Eur. J.* **2011**, *17*, 9326.

(13) Braida, B.; Hendrickx, K.; Domin, D.; Dinnocenzo, J. P.; Hiberty, P. C. *J. Chem. Theory Comput.* **2013**, *9*, 2276.

(14) Although using a minimum (2,2) active space, the nature of the bond can be qualitatively described as a "2-e/4-c" bond (see ref 6). It is also stated that long, multicenter bonds can be defined as a resonating combination of classical 3-e bonds, leading to a "6-e/4-c" description (see ref 13).

(15) (a) Tian, Y.-H.; Kertesz, M. *J. Phys. Chem. A* **2011**, *115*, 13942. (b) Shaik, S.; Danovich, D.; Wu, W.; Hiberty, P. C. *Nature Chem.* **2009**, *1*, 443. (c) Shaik, S.; Danovich, D.; Silvi, B.; Lauvergnat, D. L.; Hiberty, P. C. *Chem.—Eur. J.* **2005**, *11*, 6358.

(16) Tian, Y.-H.; Kertesz, M. *J. Am. Chem. Soc.* **2010**, *132*, 10648.

(17) (a) Capdevila-Cortada, M.; Novoa, J. J. *Chem.—Eur. J.* **2012**, *18*, 5335. (b) Fumanal, M.; Capdevila-Cortada, M.; Miller, J. S.; Novoa, J. J. *J. Am. Chem. Soc.* **2013**, *135*, 13814. (c) Spruell, J. M.; Coskun, A.; Friedman, D. C.; Forgan, R. S.; Sarjeant, A. A.; Trabolsi, A.; Fahrenbach, A. C.; Barin, G.; Paxton, W. F.; Dey, S. K.; Olson, M. A.; Benitez, D.; Tkatchouk, E.; Colvin, M. T.; Carmielli, R.; Caldwell, S. T.; Rosair, G. M.; Hewage, S. G.; Duclairoir, F.; Seymour, J. L.; Slawin, A. M. Z.; Goddard, W. A., III; Wasielewski, M. R.; Cooke, G.; Stoddart, J. F. *Nature Chem.* **2010**, *2*, 870. (d) Ferron, C. C.; Delgado, M. C. R.; Hernandez, V.; Navarrete, J. T. L.; Vercelli, B.; Zotti, G.; Cortada, M. C.; Novoa, J. J.; Niu, W.; He, M.; Hartl, F. *Chem. Commun.* **2011**, *47*, 12622.

(18) Coskun, A.; Spruell, J. M.; Barin, G.; Fahrenbach, A. C.; Forgan, R. S.; Colvin, M. T.; Carmieli, R.; Benítez, D.; Tkatchouk, E.; Friedman, D. C.; Sarjeant, A. A.; Wasielewski, M. R.; Goddard, W. A., III; Stoddart, J. F. *J. Am. Chem. Soc.* **2011**, *133*, 4538.

(19) (a) Tateno, M.; Takase, M.; Iyoda, M.; Komatsu, K.; Nishinaga, T. *Chem.—Eur. J.* **2013**, *19*, 5457. (b) Nishinaga, T.; Kageyama, T.; Koizumi, M.; Ando, K.; Takase, M.; Iyoda, M. *J. Org. Chem.* **2013**, *78*, 9205.

(20) (a) Garcia-Yoldi, I.; Miller, J. S.; Novoa, J. J. *J. Phys. Chem. A* **2009**, *113*, 7124. (b) Garcia-Yoldi, I.; Miller, J. S.; Novoa, J. J. *Phys. Chem. Chem. Phys.* **2008**, *10*, 4106. (c) Huang, J.; Kingsbury, S.; Kertesz, M. *Phys. Chem. Chem. Phys.* **2008**, *10*, 2625.

(21) Sherril, C. D.; Lee, M. S.; Head-Gordon, M. *Chem. Phys. Lett.* **1999**, *302*, 425.

(22) Benberu, H. Z.; Tian, Y.-H.; Kertesz, M. *Phys. Chem. Chem. Phys.* **2012**, *14*, 10713.

(23) Steinmann, S. N.; Corminboeuf, C. *J. Chem. Theory Comput.* **2012**, *8*, 4305.

(24) (a) Guasch, J.; Grisanti, L.; Lloveras, V.; Vidal-Gancedo, J.; Souto, M.; Morales, D. C.; Vilaseca, M.; Sissa, C.; Painelli, A.; Ratera, I.; Rovira, C.; Veciana, J. *Angew. Chem., Int. Ed.* **2012**, *51*, 1. (b) Barin, G.; Coskun, A.; Friedman, D. C.; Olson, M. A.; Colvin, M. T.; Carmielli, R.; Dey, S. K.; Bozdemir, O. A.; Wasielewski, M. R.; Stoddart, J. F. *Chem.—Eur. J.* **2011**, *17*, 213.

(25) (a) Perdew, J. P.; Burke, K.; Ernzerhof, M. *Phys. Rev. Lett.* **1996**, *77*, 3865. (b) Perdew, J. P.; Burke, K.; Ernzerhof, M. *Phys. Rev. Lett.* **1997**, *78*, 1396.

(26) (a) Becke, A. D. *Phys. Rev. A* **1988**, *38*, 3098. (b) Perdew, J. P. *Phys. Rev. B* **1986**, *33*, 8822.

(27) (a) Becke, A. D. *J. Chem. Phys.* **1993**, *98*, 5648. (b) Lee, C. T.; Yang, W. T.; Parr, R. G. *Phys. Rev. B* **1988**, *37*, 785.

(28) Becke, A. D. *J. Chem. Phys.* **1993**, *98*, 1372.

(29) Boese, A. D.; Martin, J. M. L. *J. Chem. Phys.* **2004**, *121*, 3405.

(30) Yanai, T.; Tew, D.; Handy, N. *Chem. Phys. Lett.* **2004**, *393*, 51.

(31) Krukau, A. V.; Vydrov, O. A.; Izmaylov, A. F.; Scuseria, G. E. *J. Chem. Phys.* **2006**, *125*, 224106.

(32) Chai, J.-D.; Head-Gordon, M. *J. Chem. Phys.* **2008**, *128*, 084106.

(33) Grimme, S. *J. Comput. Chem.* **2006**, *27*, 1787.

(34) Grimme, S.; Antony, J.; Ehrlich, S.; Krieg, H. *J. Chem. Phys.* **2010**, *132*, 154104.

(35) Grimme, S.; Ehrlich, S.; Georigk, L. *J. Comput. Chem.* **2011**, *32*, 1456.

(36) Zhao, Y.; Truhlar, D. G. *J. Chem. Phys.* **2006**, *125*, 194101.

(37) Zhao, Y.; Truhlar, D. G. *Theor. Chem. Acc.* **2008**, *120*, 215.

(38) Peverati, R.; Truhlar, D. G. *J. Phys. Chem. Lett.* **2011**, *2*, 2810.

(39) Grimme, S. *J. Chem. Phys.* **2006**, *124*, 034108.

(40) (a) Murray, C. W.; Handy, N. C.; Laming, G. J. *Mol. Phys.* **1993**, *78*, 997. (b) Lebedev, V. I.; Laikov, D. N. *Dokl. Math.* **1999**, *59*, 477.

(41) Chai, J.-D.; Head-Gordon, M. *Phys. Chem. Chem. Phys.* **2008**, *10*, 6615.

(42) The restricted active space is defined as follows: number of electrons in all RAS space, maximum number of holes in RAS1, and maximum number of particles in RAS3 and orbitals in RAS1, orbitals in RAS2, and orbitals in RAS3.

(43) TCNE: (a) Milián, B.; Pou-Amérigo, R.; Merchán, M.; Orti, E. *ChemPhysChem* **2005**, *6*, 503. TTF: (b) Pou-AméRigo, R.; Orti, E.; Merchán, M.; Rubio, M.; Viruela, P. *J. Phys. Chem. A* **2002**, *106*, 631.

(44) Dietchfield, R.; Hehre, W. J.; Pople, J. A. *J. Chem. Phys.* **1971**, *54*, 724.

(45) Boys, S. F.; Bernardi, F. *Mol. Phys.* **1970**, *19*, 553.

(46) (a) Beebe, N. H. F.; Linderberg, J. *Int. J. Quantum Chem.* **1977**, *7*, 683. (b) Røeggen, I. R.; Wisløff-Nielsen, E. *Chem. Phys. Lett.* **1986**,

132, 154. (c) Koch, H.; Sánchez de Merás, A.; Pedersen, T. B. *J. Chem. Phys.* **2003**, *118*, 9481.
(47) Frisch, M. J.; Trucks, G. W.; Schlegel, H. B.; Scuseria, G. E.; Robb, M. A.; Cheeseman, J. R.; Scalmani, G.; Barone, V.; Mennucci, B.; Petersson, G. A.; Nakatsuji, H.; Caricato, M.; Li, X.; Hratchian, H. P.; Izmaylov, A. F.; Bloino, J.; Zheng, G.; Sonnenberg, J. L.; Hada, M.; Ehara, M.; Toyota, K.; Fukuda, R.; Hasegawa, J.; Ishida, M.; Nakajima, T.; Honda, Y.; Kitao, O.; Nakai, H.; Vreven, T.; Montgomery, J. A., Jr.; Peralta, J. E.; Ogliaro, F.; Bearpark, M.; Heyd, J. J.; Brothers, E.; Kudin, K. N.; Staroverov, V. N.; Kobayashi, R.; Normand, J.; Raghavachari, K.; Rendell, A.; Burant, J. C.; Iyengar, S. S.; Tomasi, J.; Cossi, M.; Rega, N.; Millam, N. J.; Klene, M.; Knox, J. E.; Cross, J. B.; Bakken, V.; Adamo, C.; Jaramillo, J.; Gomperts, R.; Stratmann, R. E.; Yazyev, O.; Austin, A. J.; Cammi, R.; Pomelli, C.; Ochterski, J. W.; Martin, R. L.; Morokuma, K.; Zakrzewski, V. G.; Voth, G. A.; Salvador, P.; Dannenberg, J. J.; Dapprich, S.; Daniels, A. D.; Farkas, Ö.; Foresman, J. B.; Ortiz, J. V.; Cioslowski, J.; Fox, D. J. Gaussian 09, Revision D.01; Gaussian, Inc., Wallingford, CT, 2009.
(48) Aquilante, F.; De Vico, L.; Ferré, N.; Ghigo, G.; Malmqvist, P.-Å.; Neogrády, P.; Pedersen, T. B.; Pitonak, M.; Reiher, M.; Roos, B. O.; Serrano-Andrés, L.; Urban, M.; Veryazov, V.; Lindh, R. *J. Comput. Chem.* **2010**, *31*, 224.
(49) Note that the positive sign of this interaction means that the dimer is less stable than the dissociated monomers.
(50) The (6,4) complete active space involves 10 determinants, while the (22,2,2;10,2,8) and the (22,2,2;8,4,8) restricted active spaces involve 28,290 and 91,750 determinants, respectively.
(51) The (14,12) complete active space involves 314,028 determinants, while the (30,2,2;14,2,12) restricted active space involves 120,526 determinants.